JCTC Journal of Chemical Theory and Computation

Article

pubs.acs.org/JCTC

Vibrational Circular Dichroism Spectra for Large Molecules through Molecules-in-Molecules Fragment-Based Approach

K. V. Jovan Jose, Daniel Beckett, and Krishnan Raghavachari*

Department of Chemistry, Indiana University, Bloomington, Indiana 47405, United States

Supporting Information

ABSTRACT: We present the first implementation of the vibrational circular dichroism (VCD) spectrum of large molecules through the Molecules-in-Molecules (MIM) fragment-based method. An efficient projection of the relevant higher energy derivatives from smaller fragments to the parent molecule enables the extension of the MIM method for the evaluation of VCD spectra (MIM-VCD). The overlapping primary subsystems in this work are constructed from interacting fragments using a number-based scheme and the dangling bonds are saturated with link hydrogen atoms. Independent fragment calculations are performed to evaluate the energies, Hessian matrix, atomic polar tensor (APT), and the atomic axial tensor (AAT). Subsequently, the link atom tensor components are projected back onto the corresponding host and supporting atoms through the Jacobian projection method, as in the ONIOM approach. In the two-layer model, the long-range interactions between fragments are accounted for using a less computationally intensive lower level of theory. The performance of the MIM model is calibrated on the D- and L-enantiomers of 10 carbohydrate benchmark molecules, with strong intramolecular interactions. The vibrational frequencies and VCD intensities are accurately reproduced relative to the full, unfragmented, results for these systems. In addition, the MIM-VCD method is employed to predict the VCD spectra of perhydrotriphenylene and cryptophane-A, yielding spectra in agreement with experiment. The accuracy and performance of the benchmark systems validate the MIM-VCD model for exploring vibrational circular dichroism spectra of large molecules.

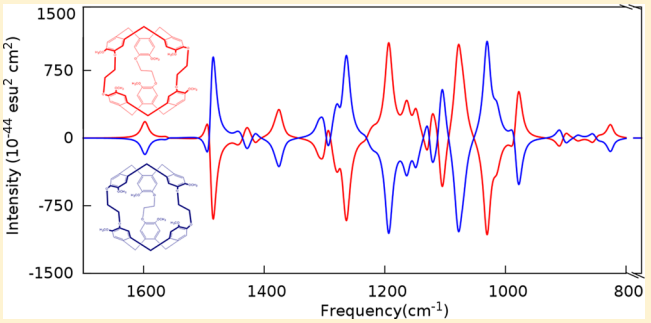

1. INTRODUCTION

Determining the absolute configuration of a chiral system is critical in understanding molecular structure−activity relationships. For example, the enantiomers of a chiral molecule often exhibit significantly different pharmacological and toxicological effects. In principle, the absolute configuration of a chiral molecule can be determined by stereocontrolled organic synthesis or by techniques such as X-ray diffraction (XRD) and nuclear magnetic resonance (NMR).[1] However, synthesizing high-quality crystals for XRD, or preparing a diastereomer with shift reagent for NMR studies, can be laborious or impossible. An alternative practical strategy to determine absolute configurations is via chiral vibrational spectroscopies such as vibrational circular dichroism (VCD) and Raman optical activity (ROA). VCD characterizes the differential absorption of left and right circularly polarized infrared (IR) radiation by chiral molecules. Enantiomers exhibit VCD spectra with intensities of the same magnitude but opposite signs. VCD[2] and ROA[3,4] are the most effective and reliable techniques for predicting absolute configurations that may not be easily accessible through other spectroscopic methods.[5−8]

VCD is an intrinsically weak phenomenon, the circular differential absorption being several orders of magnitude weaker than the corresponding vibrational infrared absorption. Yet, accurate VCD measurements are possible due to advances in VCD instrumentation. However, unambiguous interpretation of experimental VCD spectra is hindered by the difficulty of establishing a direct relationship between observed spectra and molecular structure.[9] At this juncture, the combination of accurate quantum chemical calculations and experimental VCD measurements offers a robust approach for the determination of the absolute configurations of chiral molecules.[10−12] Indeed, there are many systems that have been explored theoretically and experimentally.[13] However, the computation of VCD spectra involves the evaluation of higher derivatives of the energy that can be computationally demanding. In addition, it is known that fairly large basis sets including diffuse and polarization functions are needed to assign experimental VCD spectra reliably.[13] The high scaling of these methods can limit the applicability of direct *ab initio* VCD spectral calculations for large systems.

Significant progress in the quantum mechanical studies of large molecules in the past decade has come from the development of fragment-based methods for the fast evaluation of the total energies.[14] The basic idea involved in these methods is to generate a set of subsystems and assemble their

Received: July 7, 2015

DOI: 10.1021/acs.jctc.5b00647
J. Chem. Theory Comput. XXXX, XXX, XXX−XXX

subsystem energies in a systematic way to construct the total energy of the large molecule. Although there are many such methods for evaluating the energies, the corresponding derivative expressions needed for the calculation of higher-order molecular properties such as VCD are not available in most fragment-based methods.

We have recently proposed a new hybrid extrapolation method called Molecules-in-Molecules (MIM).[15] MIM employs a multilayer partitioning technique with multiple levels of theory using a generalized hybrid energy expression, similar in spirit to ONIOM. The steps involved in MIM are (1) selection of nonoverlapping fragments by cutting appropriate covalent bonds in the large molecule, (2) formation of overlapping primary subsystems by allowing the fragments to interact with neighboring fragments based on a well-defined scheme (distance, connectivity, or number-based, *vide infra*), (3) formation of derivative subsystems to take into account the overcounting of the regions in the primary subsystems, and (4) summation of the energies of the primary and derivative subsystems (after link atom termination of the broken covalent bonds and taking into account the appropriate signs of the energy terms). Most importantly, the use of multiple layers with different levels of theory makes it an efficient extrapolation method, compared to many fragment-based methods that use a single layer.

The performance of the MIM model has previously been validated for accurate energy evaluations and infrared vibrational spectra of large chemical systems such as oligopeptides.[16] In particular, the two-layer MIM model (MIM2) was shown to be more effective than a single layer model (MIM1) for the evaluation of accurate infrared vibrational spectra. Since the long-range interactions in MIM2 are accounted for at a low level of theory, the fragment size at the high level of theory can be kept reasonably small. In the present work, we have extended this method to evaluate the Hessian, atomic polar tensors, and atomic axial tensors for the precise evaluation of the VCD spectra of large molecules.

The following sections of the current paper are organized as follows. Section 2 describes the theoretical background for VCD calculations and our procedure involved for evaluating MIM energies and their higher derivatives. Section 3 presents a benchmark analysis of MIM-VCD spectra on 10 carbohydrate molecules, as well as a comparison with experiment for two larger molecules: perhydrotriphenylene and cryptophane-A. Section 4 compares our approach with previous approaches used for large molecules. Section 5 provides a summary and conclusions.

2. COMPUTATIONAL METHODS AND THEORY

VCD is defined as the differential absorbance (ΔA) of left (A_L) and right (A_R) circularly polarized electromagnetic radiation in the infrared region. Unlike the vibrational absorbance spectra, the VCD band intensity can be either positive or negative, depending on the difference in absorbance. Enantiomers have intensity bands that are equal in magnitude but opposite in sign. Hence, the VCD spectra can distinguish the absolute configuration of chiral molecules.

The theory and implementation aspects of VCD spectral evaluations have been extensively discussed previously.[17−24] Here we follow the approach pioneered by Stephens and coworkers,[13] using magnetic field perturbation theory. Briefly, the effect of the electromagnetic radiation on the molecule is given as a perturbing contribution:

$$H'(E, H) = -\mu_{ele}\cdot E - \mu_{mag}\cdot H \tag{1}$$

where μ_{ele} and μ_{mag} refer to the electric and magnetic dipole moment operators, respectively. Under time-dependent perturbation theory, the integrated VCD band intensity of the fundamental vibrational excitation, viz., from 0 → 1, within the ground electronic state, is determined by the rotational strength.[1]

$$R_{0\to 1}(i) = Im[\langle 0|\mu_{ele}|1\rangle_i \cdot \langle 1|\mu_{mag}|0\rangle_i] \tag{2}$$

The VCD intensity of the ith normal mode is thus proportional to the imaginary part of the scalar product of the electric-dipole transition moment and the magnetic dipole transition moment. The VCD intensity can be thought of as determined by the angle between the electric dipole and magnetic dipole transition moments, $\langle 0|\mu_{ele}|1\rangle_i$ and $\langle 1|\mu_{mag}|0\rangle_i$, respectively. If these two vectors are orthogonal, as in achiral molecules, the rotational strength is zero.

For the computation of the rotational strength, the transition moments are defined by two tensors for each atom, λ: the atomic polar tensor (APT), $P^{\lambda}_{\alpha\beta}$ and the atomic axial tensor (AAT), $M^{\lambda}_{\alpha\beta}$. The alpha and beta subscripts label the components in Cartesian directions X, Y, or Z. The APT corresponds to the electric transition dipole moment, and the AAT corresponds to the magnetic transition dipole moment. While the former is relatively straightforward and is needed for the evaluation of infrared vibrational absorption, the latter, being an imaginary perturbation, is more complicated.

Within the Born−Oppenheimer approximation, the dipole moment operator can be expanded up to first order, in terms of the mass-weighted normal coordinate (Q_i), and the electric transition dipole moment for the ith normal mode is given by

$$\langle 0|\mu_{ele}|1\rangle_i = \left(\frac{\partial \mu^{G}_{ele}}{\partial Q_i}\right)\left(\frac{\hbar}{4\pi\nu_i}\right)^{1/2} \tag{3}$$

Here, μ^{G}_{ele} is the electric dipole moment of the ground electronic state, and $((\partial\mu^{G}_{ele})/(\partial Q_i))$ is the first derivative with respect to the normal coordinate, Q_i, at the equilibrium geometry. The corresponding dipole absorption strength of the ith fundamental vibrational transition is the square of the electric transition dipole moment and is given as

$$D_{0\to 1}(i) = \left(\frac{\partial \mu^{G}_{ele}}{\partial Q_i}\right)^2\left(\frac{\hbar}{4\pi\nu_i}\right) \tag{4}$$

Using the transformation between the normal coordinate and the Cartesian displacement coordinate, $X_{\lambda\alpha} = \sum_i S_{\lambda\alpha,i}Q_i$, this can be expressed as

$$D_{0\to 1}(i) = \left(\frac{\hbar}{4\pi\nu_i}\right)\sum_{\beta}\sum_{\substack{\lambda,\alpha\\ \lambda',\alpha'}}[S_{\lambda\alpha,i}P^{\lambda}_{\alpha\beta}][S_{\lambda'\alpha',i}P^{\lambda'}_{\alpha'\beta}] \tag{5}$$

The tensor $P^{\lambda}_{\alpha\beta}$ is known as the atomic polar tensor (APT) and represents the derivative of the molecular electric dipole moment with respect to the Cartesian displacement of the λth atom at equilibrium.

$$P^{\lambda}_{\alpha\beta} = \left(\frac{\partial \mu^{G}_{\beta}}{\partial X_{\lambda\alpha}}\right)_0 = \frac{\partial^2 E}{\partial X_{\lambda\alpha}\partial F_{\beta}} \tag{6}$$

DOI: 10.1021/acs.jctc.5b00647
J. Chem. Theory Comput. XXXX, XXX, XXX−XXX

Being a square as in eq 4, the infrared absorption intensity is always positive.

The magnetic transition dipole behaves differently than the electric transition dipole. Within the Born−Oppenheimer approximation, the magnetic dipole transition moment is zero (for a nondegenerate electronic state). Thus, a more sophisticated treatment is needed involving a mixing with the excited electronic states using perturbation theory. The resulting equation for the magnetic dipole transition moment of the fundamental ith normal mode can be expressed as

$$\langle 0|\mu_{\mathrm{mag}}|1\rangle_i = (4\pi\hbar^3\upsilon_i)^{1/2} \sum_{\lambda,\alpha} S_{\lambda\alpha,i} M^{\lambda}_{\alpha\beta} \tag{7}$$

Here, $M^{\lambda}_{\alpha\beta}$ is a second-rank tensor termed the atomic axial tensor (AAT) and represents the derivative of the molecular magnetic dipole moment with respect to the Cartesian displacement of the λth atom at equilibrium. While the details of the derivation are not discussed, the electronic part of the magnetic transition moment contains terms involving the derivatives of the ground-state wave function with respect to the Cartesian displacement coordinates, as well as the external magnetic field. The latter term is also needed in the evaluation of the nuclear magnetic shielding tensors for the calculation of the NMR spectra of molecules. After the determination of $M^{\lambda}_{\alpha\beta}$, the rotational strength can be calculated as

$$R_{0\to 1}(i) = \hbar^2 \sum_{\beta} \sum_{\substack{\lambda,\alpha \\ \lambda',\alpha'}} [S_{\lambda\alpha,i} P^{\lambda}_{\alpha\beta}][S_{\lambda'\alpha',i} M^{\lambda'}_{\alpha'\beta}] \tag{8}$$

In summary, the prediction of VCD spectra within the harmonic approximation requires (a) evalutation of the second derivatives of the energy with respect to the nuclear displacement coordinates (i.e., the Hessian matrix that yields the harmonic vibrational frequencies), and (b) calculation of the VCD intensity through the evaluation of the APT and AAT. The first-principles evaluation of these terms is the most difficult in the calculation of the VCD spectrum. This can be a bottleneck for the evaluation of the VCD spectra for large molecules, particularly when used in conjunction with large basis sets.

We now outline the fragment-based strategy for the efficient evaluation of VCD spectra for large molecules. The current section details the computational procedure, as well as the method used for the accurate estimation of the electronic energy, molecular geometry, Hessian matrix, and atomic axial and atomic polar tensors through the MIM procedure. All the actual and MIM calculations are carried out using the Gaussian program suite.[25] MIM fragmentation schemes and VCD evaluations are implemented through an external Perl script interface.

(1) The MIM procedure for evaluation of VCD spectra begins with the generation of the fragments by cutting only the C−C single bonds in the large molecule. The primary subsystems are then assembled from the interacting fragments through a number-based scheme (involving trimer units, *vide infra*). All the dangling bonds in the subsystems are saturated with hydrogen link atoms. The link atoms are placed along the vector connecting the supporting and host atoms at a distance defined through a linear equation, $R_2 = R_1 + g(R_3 - R_1)$, with a scale factor, g.[26] Here, R_2, R_1, and R_3 are the Cartesian components of link, supporting, and host atoms, respectively. The scale factor is dependent on the nature of the bond being cut while constructing a model system from the real system as in the standard ONIOM method.[26] The subsystems are then used to evaluate the total energy and its derivatives.

(2) The total energy of the system in a two-layer MIM model (MIM2) can be constructed from the subsystem energies through a generalization starting from the two-layer ONIOM extrapolation expression

$$E_{\mathrm{total}} = E_{\mathrm{rl}} - E_{\mathrm{ml}} + E_{\mathrm{mh}} \tag{9}$$

Here, the energy of the model region calculated at a low level of theory (E_{ml}) is subtracted from the energy of the real (i.e., full) system calculated at the low level (E_{rl}). The energy of the model system is then calculated at a high level of theory (E_{mh}) and added in, to obtain the extrapolated total ONIOM energy. However, unlike standard ONIOM, which contains only one model system, the full system in MIM involves overlapping subsystems that can each be considered as a model system. The overcounting of the overlapping regions of the primary subsystems is taken into account via derivative subsystems by means of the inclusion−exclusion principle. It is convenient to redefine the energies of model-high (E_{mh}) and model-low (E_{ml}) levels of theory as a sum over all the subsystems as follows:

$$E_{\mathrm{ml/mh}} = \sum_i E^i_{\mathrm{l/h}} - \sum_{ij} E^{i\cap j}_{\mathrm{l/h}} + \cdots + (-1)^{n-1} \sum_n E^{i\cap j\cap k\cdots\cap n}_{\mathrm{l/h}} \tag{10}$$

Here, $E^i_{\mathrm{l/h}}$ represents the energy of the ith primary subsystem (at the low or high level of theory), while the other terms involving the overlapping terms represent the derivative subsystems. It is important to note that the redefined "model-high" and "model-low" levels in MIM extend through the entire molecule via summation over the subsystems.

(3) Within MIM2, the link atom force components are projected back onto the supporting and host atoms through a general Jacobian projection method,[26] as

$$F_a = \frac{\partial E_{\mathrm{total}}}{\partial X_a} = \frac{\partial E_{\mathrm{rl}}}{\partial X_a} - \sum_{L=1}^{M} \frac{\partial E_{\mathrm{ml}}}{\partial X_a} J(R_2; R_1, R_3) + \sum_{L=1}^{M} \frac{\partial E_{\mathrm{mh}}}{\partial X_a} J(R_2; R_1, R_3) \tag{11}$$

Here, the index a corresponds to the Cartesian components in the X, Y, or Z directions. The forces can be used to perform a fragment-based geometry optimization procedure, as already described in our previous work.[16]

(4) At the optimized geometry, the mass-weighted Hessian of link atom is projected back onto the supporting and host atoms through the general expression

$$H_{ab} = \frac{\partial^2 E_{\mathrm{total}}}{\partial X_\alpha \partial X_\beta} = \frac{\partial^2 E_{\mathrm{rl}}}{\partial X_\alpha \partial X_\beta} - \sum_{L=1}^{M} J^{\mathrm{T}} \frac{\partial^2 E_{\mathrm{ml}}}{\partial X_\alpha \partial X_\beta} J + \sum_{L=1}^{M} J^{\mathrm{T}} \frac{\partial^2 E_{\mathrm{mh}}}{\partial X_\alpha \partial X_\beta} J \tag{12}$$

The Hessian matrix elements, H_{ab}, which are modified by the link atom Jacobi-projection, are the blocks of elements involving link atom indices. More details are given in our previous paper on the evaluation of IR spectra with MIM2.[16]

(5) In MIM, the electronic contribution to the APT for evaluating the VCD intensity is constructed from the separate

DOI: 10.1021/acs.jctc.5b00647
J. Chem. Theory Comput. XXXX, XXX, XXX−XXX

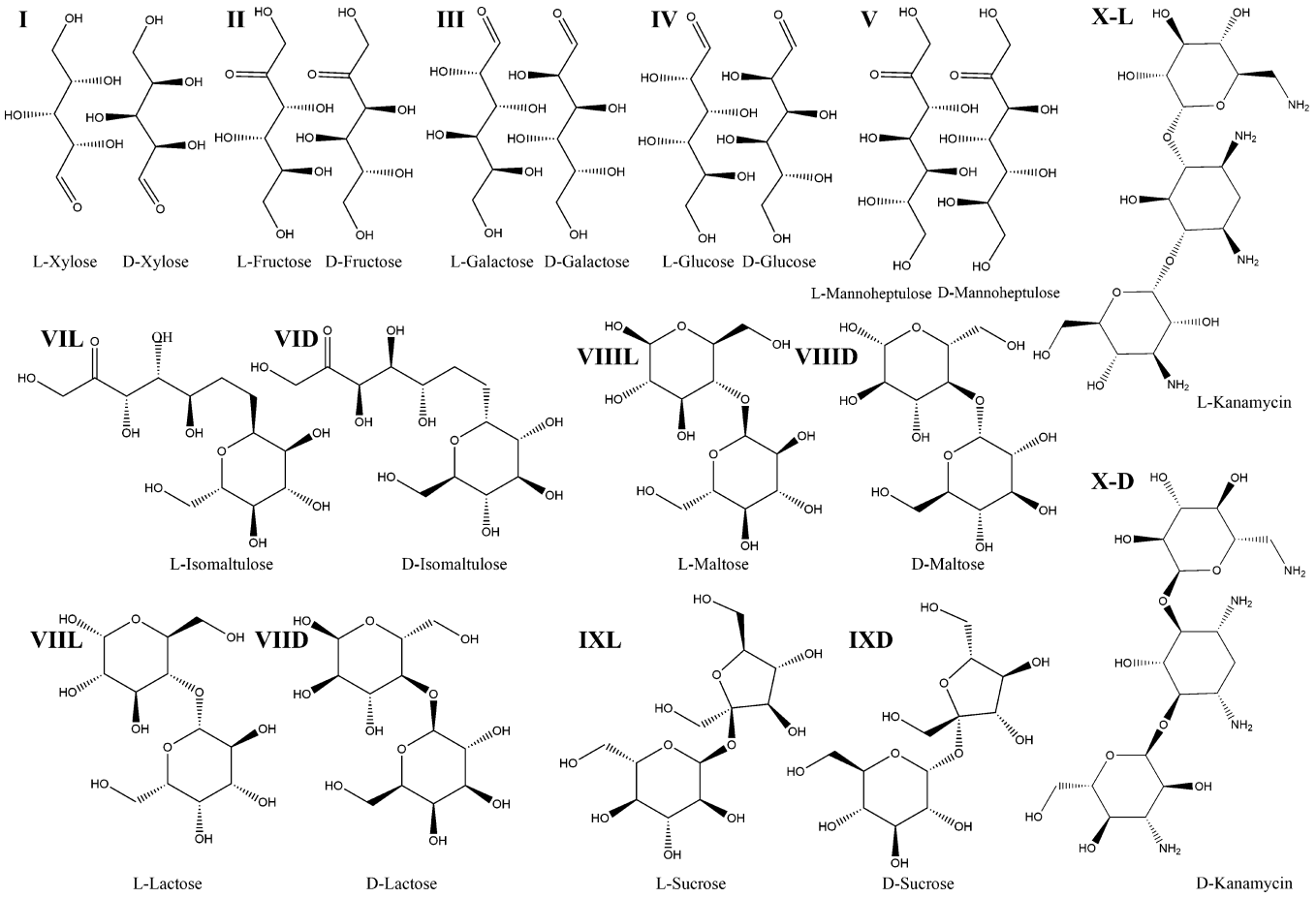

Figure 1. Set of D and L carbohydrate molecules employed for benchmarking the MIM-VCD method. An analyses of the energies and VCD spectra of structures IL-XL are reported in Table 1. Optimized geometries and full VCD spectra are furnished in Table S1 in the Supporting Information. See the text for more details.

fragment calculations through the general extrapolation expression

$$P^{\lambda}_{\alpha\beta,\mathrm{total}} = \frac{\partial^2 E_{\mathrm{total}}}{\partial X_{\lambda\alpha}\partial F_{\beta}} = P^{\lambda}_{\alpha\beta,\mathrm{rl}} - \sum_{L=1}^{M} P^{\lambda}_{\alpha\beta,\mathrm{ml}} J(R_2;\, R_1,\, R_3) + \sum_{L=1}^{M} P^{\lambda}_{\alpha\beta,\mathrm{mh}} J(R_2;\, R_1,\, R_3) \quad (13)$$

The individual expression for the atomic polar tensor is defined as in eq 6.

(6) Similarly, the electronic contribution to the AAT is constructed through the general extrapolation expression

$$M^{\lambda}_{\alpha\beta,\mathrm{total}} = M^{\lambda}_{\alpha\beta,\mathrm{rl}} - \sum_{L=1}^{M} M^{\lambda}_{\alpha\beta,\mathrm{ml}} J(R_2;\, R_1,\, R_3) + \sum_{L=1}^{M} M^{\lambda}_{\alpha\beta,\mathrm{mh}} J(R_2;\, R_1,\, R_3) \quad (14)$$

To summarize, the procedure starts with the initial determination of the optimized molecular geometry, using the fragment-based energy gradients. The mass-weighted Hessian is then diagonalized to evaluate the vibrational normal mode frequencies, and the APT and AAT from eqs 13 and 14 are employed to evaluate the rotational strengths and the VCD intensities. The use of gauge-invariant atomic orbitals ensures that the resulting rotational strengths are origin-independent.

The above implementation of the algorithm is general and will work with any arbitrary fragmentation scheme at the primary level. In the present work, we have taken into account 10 prototype carbohydrate molecules for benchmarking the MIM method. The initial nonoverlapping fragments are constructed by breaking the backbone C−C single bonds of the benchmark molecules. The interacting fragments are combined, employing a number-based criterion (mostly using trimer units) based on the connectivity information, for constructing the overlapping primary subsystems. An example illustrating dimer- and trimer-based fragmentation schemes used for D-sucrose is illustrated in Figure S1 in the Supporting Information. These primary subsystems can be constructed through a systematic procedure applicable to more-complex chemical systems. The derivative subsystems are then constructed from the primary subsystems via the inclusion−exclusion principle. While the current description involves the use of hydrogen link atoms to saturate the broken covalent bonds, the same method can be applied with minor modifications for molecular clusters where no link atoms are involved while constructing fragments. Finally, the above-mentioned MIM procedure for performing the geometry optimization and evaluating vibrational spectra of a molecule is independent of the levels of theory and basis sets.

DOI: 10.1021/acs.jctc.5b00647
J. Chem. Theory Comput. XXXX, XXX, XXX−XXX

3. RESULTS AND DISCUSSION

To assess the accuracy and applicability of MIM-VCD, a careful benchmark study is performed for the D- and L-forms of 10 medium- to large-sized carbohydrate molecules. There are many chiral centers in these molecules and show specific characteristics in the VCD spectrum, making them attractive systems for benchmarking. The agreement between MIM-VCD and directly evaluated (i.e., unfragmented) VCD spectra is discussed for these systems in section 3.1. In the next assessment, the MIM-VCD spectrum of a chiral hydrocarbon system, perhydrotriphenylene, is compared with the experimental spectrum and with previous work[27] in section 3.2. The final section, section 3.3, presents a comparative analysis of MIM-VCD spectrum with the experimental spectrum for a large molecule that has been well-studied previously: cryptophane-A.[28]

3.1. Comparison of MIM-VCD with Full Calculations.

The D- and L-forms of the 10 benchmark carbohydrate molecules are depicted in Figures 1 and 2. The first five molecules are simple monosaccharides and were calculated in their acyclic form for benchmarking purposes, while the last five molecules are sufficiently more complicated and were calculated in their most stable geometries. The associated structure numbers are used consistently to identify the systems throughout the text, as well as in all figures and tables. These calibration studies are carried out using density functional theory at the B3LYP/6-311+G(d,p) level of theory. For MIM2, we have employed a second layer at both HF/6-31G(d) and B3LYP/6-31G(d) levels of theory for correcting the molecular properties. These results are compared with the actual calculations performed at B3LYP/6-311+G(d,p) levels of theory. The entries in the bracket following "MIM" give the level(s) of theory and basis set(s) employed for the calculations. The geometry optimizations are performed on the test systems (as described in the Computational Methods and Theory section) at three different combinations of levels of theory: (1) MIM1[B3LYP/6-311+G(d,p)], (2) MIM2-[B3LYP/6-311+G(d,p):HF/6-31G(d)], and (3) MIM2-[B3LYP/6-311+G(d,p):B3LYP/6-31G(*d*)]. For simplicity, they will be denoted as MIM1, MIM2(HF), and MIM2-(B3LYP) in this subsection. The VCD spectra evaluated at these levels of theory are compared with the corresponding full unfragmented calculations (referred to as "actual") at B3LYP/6-311+G(d,p). In previous work, we have shown that MIM reproduces the geometrical parameters of the actual high calculations very accurately with a correlation factor of ~1.0.[16] While MIM1 was quite accurate for most molecules, MIM2 performed better in reproducing the dihedral angles of larger molecules such as peptides with significant intramolecular interactions. In the case of the 10 benchmark systems, all models work very well, and we do not present an analysis of the actual and MIM geometrical parameters of these systems.

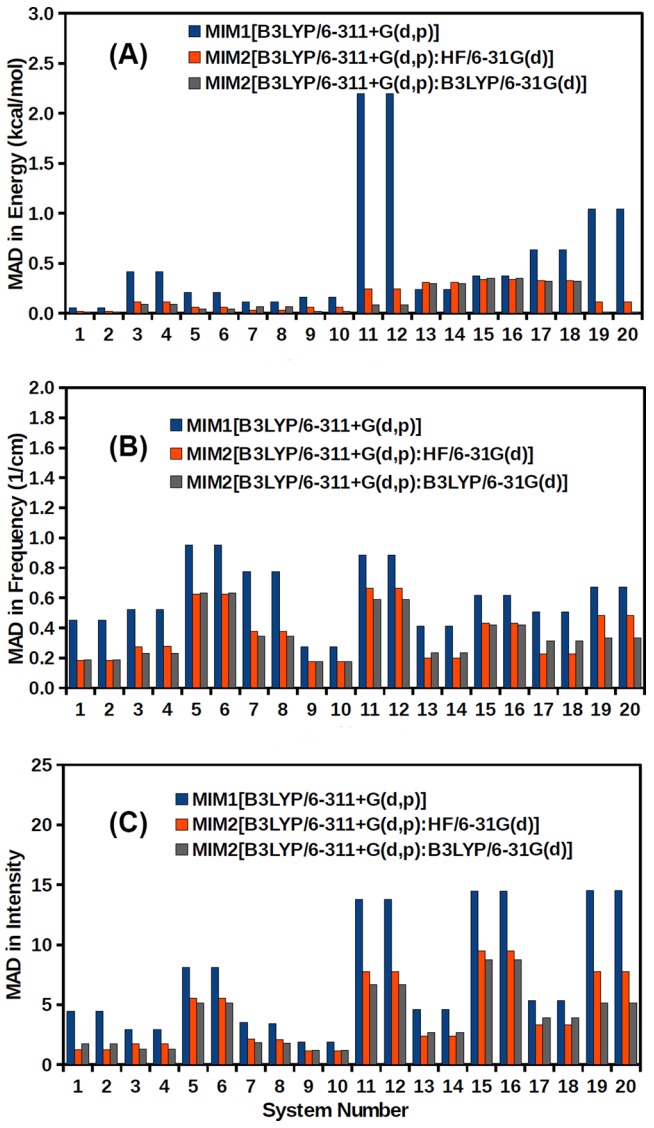

Figure 2. Bar graphs showing mean absolute deviation (MAD) in (A) energies, (B) normal mode frequencies, and (C) VCD intensities of the benchmark molecules. See the text for more details.

Table 1 presents the actual energies of the benchmark molecules, and a comparison of MIM1 and MIM2(B3LYP) energies relative to the full "actual" calculations at the B3LYP/6-311+G(d,p) level. Compared to the actual energies, the mean absolute deviations (MAD) at MIM1 and MIM2 are 0.50 and 0.11 kcal/mol, respectively. This corresponds to a 78% improvement in accuracy at MIM2 compared to MIM1. The latter improvement in accuracy demonstrates the importance of the second layer of theory in accounting for the long-range intramolecular interactions in these benchmark molecules. The next two columns in Table 1 report the two most intense VCD peaks of the benchmark molecules. In each of the benchmark systems, we have confirmed that the D and L forms yield the same total energy and vibrational frequency, while the VCD intensity changes sign. Thus, the VCD intensities are listed only for the L-enantiomers. The final columns report the MAD value of each full spectrum, including all of the $3N - 6$ normal modes at MIM1 and MIM2(B3LYP), relative to the actual spectrum. The full VCD spectra of all the benchmark stereoisomers are reported in Table S1 in the Supporting Information. The MAD at MIM2(B3LYP) shows ~43% improvement over MIM1 in frequencies and ~51% improvement in VCD intensities, consistent with the significant improvement in the energy. The average MAD in the frequencies [and intensities] over all benchmark molecules is 0.61 cm^{-1} [7.69 esu^2 cm^2] at MIM1. The corresponding improvement in MAD for MIM2(B3LYP) is 0.35 cm^{-1} [3.77 esu^2 cm^2].

A complete analysis of the MIM2 method with different combinations of levels of theory on the benchmark set is depicted in Figure 3. Once again, it is seen that the accuracy of

DOI: 10.1021/acs.jctc.5b00647
J. Chem. Theory Comput. XXXX, XXX, XXX−XXX

Table 1. Columns List Structure Number, Name, Number of Basis Functions (NBasis), Actual Energies (Hartrees), Calculated Errors in MIM1 and MIM2 Energies (kcal/mol), the Frequencies (cm^{-1}) and Intensities (10^{-44} esu^2 cm^2) of the Two Most Intense Peaks Evaluated MIM2[B3LYP/6-311+G(d,p):B3LYP/6-31G(d)], and the MAD in Frequencies and Intensities Relative to Actual[B3LYP/6-311+G(d,p)] Results[a]

			Energy			VCD Frequency[Intensity]		MAD in Frequency[Intensity]	
No.	system	NBasis	$E^{(Act)}$	ΔE^{MIM1}	ΔE^{MIM2}	ν [I_{max}^{MIM2}]	ν [I_{max}^{MIM2}]	$\Delta\nu$ [ΔI^{MIM1}]	$\Delta\nu$ [ΔI^{MIM2}]
IL	L-xylose	280	−572.82673	0.053	0.013	1137.8 [+209.1]	1210.1 [−126.0]	0.45 [4.44]	0.19 [1.72]
IIL	L-fructose	336	−687.39151	0.414	0.090	570.2 [−127.8]	1051.9 [−120.4]	0.52 [2.92]	0.23 [1.31]
IIIL	L-galactose	336	−687.38268	0.209	0.040	529.2 [−183.8]	267.7 [+154.2]	0.95 [8.12]	0.63 [5.16]
IVL	L-glucose	336	−687.38396	0.116	0.068	679.0 [−172.6]	505.6 [−162.0]	0.78 [3.53]	0.34 [1.84]
VL	L-mannoheptulose	392	−801.95258	0.163	0.019	237.7 [+211.7]	1060.1 [+207.0]	0.27 [1.89]	0.18 [1.20]
VIL	L-isomalt	638	−1298.32975	2.198	0.084	1064.6 [−577.4]	571.5 [+339.2]	0.88 [13.78]	0.59 [6.65]
VIIL	L-lactose	638	−1298.34345	0.238	0.295	1111.6 [−347.7]	1082.2 [−345.0]	0.41[4.62]	0.23 [2.67]
VIIIL	L-maltose	638	−1298.34918	0.372	0.349	1091.3 [−473.6]	408.3 [+298.0]	0.62 [14.47]	0.42 [8.74]
IXL	L-sucrose	638	−1298.34865	0.249	0.124	1057.9 [+251.6]	1109.7 [−230.4]	0.50 [8.83]	0.32 [3.24]
XL	L-kanamycin	942	−1754.55104	1.043	0.013	863.1 [−368.1]	1060.7 [+276.5]	0.67 [14.50]	0.33 [5.15]
	average			**0.506**	**0.110**			**0.61**[**7.69**]	**0.35**[**3.77**]

[a]Refer to the text for further details.

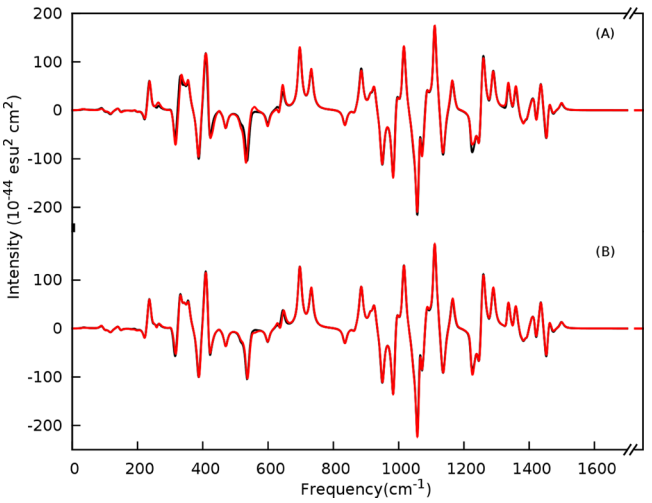

Figure 3. Comparison of actual (in black) VCD spectrum with (A) MIM1[B3LYP/6-31+G(d,p)] and (B) MIM2[B3LYP/6-31+G-(d,p):B3LYP/6-31G] spectra of D-sucrose (in red). The fragments are constructed by breaking only C−C bonds, and the primary subsystems are constructed from trimer units. See the text for more details.

the full spectrum significantly improves on incorporating a complete low level calculation as a second layer, even when it is Hartree−Fock.

To illustrate the performance of MIM-VCD, comparisons of the D-sucrose MIM-VCD vibrational spectra between 0 and 1700 cm^{-1} with the actual spectra are shown in Figures 3 and 4. In D-sucrose, the most intense peaks correspond to 1058.0 cm^{-1} [−251.6 esu^2 cm^2] and 1109.7 cm^{-1} [230.4 esu^2 cm^2]. These frequencies correspond to the C−C and C−O stretching modes, respectively. Figure 3 shows the MIM1 and MIM2-(B3LYP) spectra using primary subsystems composed of trimer units (i.e., three interacting fragments in each subsystem). The actual spectrum is shown in black, while the MIM-VCD spectrum is shown in red. The black spectrum is barely visible in the MIM2 spectrum, indicating that the agreement is essentially perfect. If a smaller, dimer unit is used to derive the primary subsystems, the corresponding spectra are shown in Figure 4. Significant deviations are now seen between the actual and MIM-VCD spectra. Thus, the more appropriate trimer-based subsystems are used for the larger systems considered below.

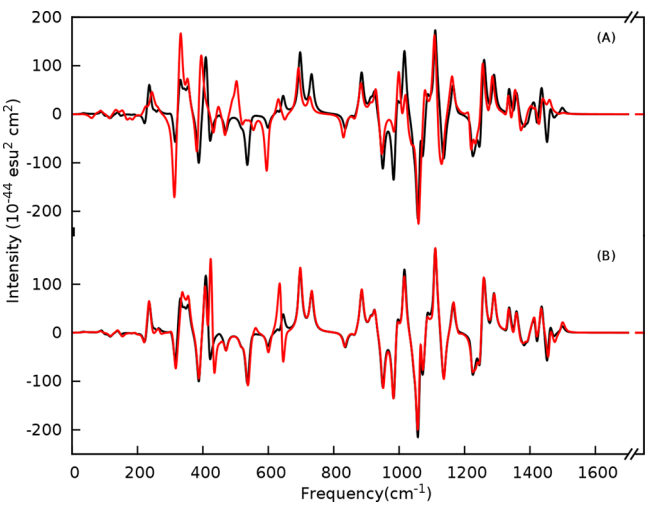

Figure 4. Comparison of actual (in black) VCD spectrum with (A) MIM1[B3LYP/6-31+G(d,p)] and (B) MIM2[B3LYP/6-31+G-(d,p):B3LYP/6-31G] spectra of D-sucrose (in red). The fragments are constructed by breaking only C−C bonds, and the primary subsystems are constructed from dimer units. See the text for more details.

3.2. Comparison of Perhydrotriphenylene MIM-VCD with Experiment. To showcase the applicability of MIM-VCD in predicting experimental spectra, we have made an explicit comparison of the calculated MIM-VCD spectra with experiment for two test systems. For the first set of experimental comparisons, we have chosen the (S)-enantiomer of D_3-anti-trans-anti-trans-anti-trans-perhydrotriphenylene (S-PHTP), shown in Figure 5 as molecule **XI-S**, which was previously investigated by Stephens et al.[27] Previous comformational analysis of perhydrotriphenylene has shown that all four cyclohexane rings in this molecule preferentially adopt a chair form over the other conformations. Hence, this stereoisomer is the most stable conformer and is effectively a rigid molecule on

DOI: 10.1021/acs.jctc.5b00647
J. Chem. Theory Comput. XXXX, XXX, XXX−XXX

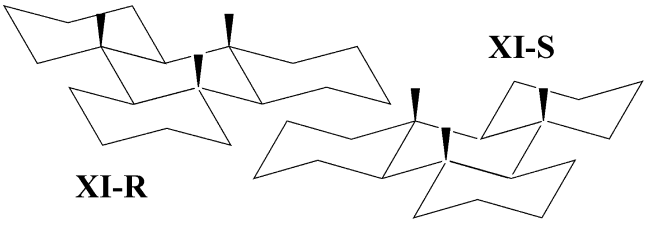

Figure 5. R- and S-enantiomers of D_3-anti-trans-anti-trans-anti-trans-perhydrotriphenylene (**XI**) employed for benchmarking the MIM-VCD method. See the text for more details.

the potential energy surface. This makes a theory-to-experiment comparison relatively straightforward because we can take into account only this most stable conformer.

Figure 6 depicts a comparison of the experimental VCD spectrum of S-PHTP[27] with the calculated MIM-VCD

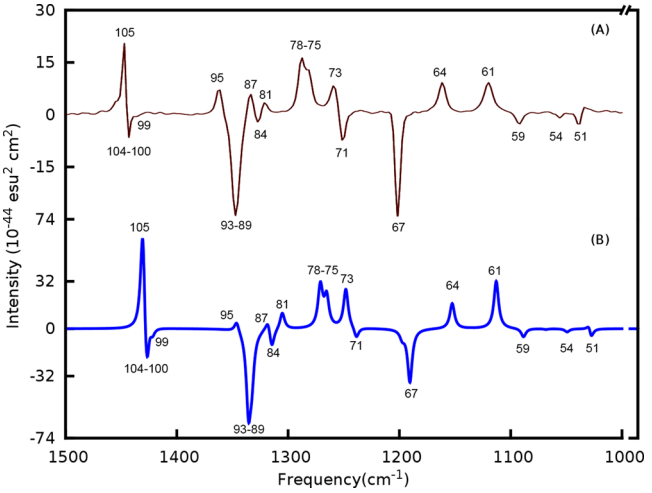

Figure 6. Comparison of (A) experimental (in brown) with (B) MIM2[MPW1PW91/aug-cc-pVTZ-f:MPW1PW91/6-31+G(d)] VCD (in blue) spectra of S-(+)-D_3-anti-trans-anti-trans-anti-trans-perhydrotriphenylene (**XI-S**). Coordinates and full VCD spectra are available in Table S2 in the Supporting Information. See the text for more details.

spectrum between 600 cm^{-1} and 1700 cm^{-1}. From previous calculations using several density functionals on some test systems, it was shown that the MPW1PW91 hybrid density functional results in the fewest number of sign errors compared to experiment.[13] Hence, in the current experimental comparison, we have employed the MPW1PW91 functional with a large aug-cc-pVTZ-f basis set at the high level and a smaller 6-31+G(d,p) basis set at the low level [MIM2[MPW1PW91/aug-cc-pVTZ-f:MPW1PW91/6-31+G(d)]. The resulting normal modes are scaled by a uniform factor of 0.971, to account for the systematic deviations, and the calculated VCD spectra using a Lorentzian line shape with a width of 3.5 cm^{-1} are depicted in Figure 6. All the $3N - 6$ (scaled) normal modes and intensities are reported in Table S2 in the Supporting Information. It is clear from Figure 6 that the calculated VCD spectrum of S-PHTP shows excellent agreement with experiment. The most important factors in deciding whether a calculated VCD spectrum agrees well with the experiment are relative peak location, relative peak magnitude, and the sign of each intensity. On these merits, both full and MIM-VCD calculations are suitable for peak assignment for perhydrotriphenylene. As seen in Figure 6, the most intense band at 1353.9 cm^{-1} [−57.5 esu^2 cm^2] corresponds to H−C−H wagging mode, and the second most intense normal mode at 1449.7 cm^{-1} [57.3 esu^2 cm^2] corresponds to the H−C−H scissoring mode.

To bring out the effects of the levels of theory and basis functions, we have carried out the VCD spectral evaluation at three more combinations of levels of theory: MIM2-[MPW1PW91/cc-pVDZ:MPW1PW91/6-31G(d)], MIM2-[B3PW91/cc-pVDZ:B3PW91/6-31G(d)], and MIM2-[B3LYP/cc-pVDZ:B3LYP/6-31G(d)]. All three combinations of these levels of theory could also reproduce the frequencies and VCD intensities very well. Our results are in excellent agreement with previous calculations reported by Stephens et al.[27]

3.3. Comparison of Cryptophane-A MIM-VCD with Experiment. As a final system to demonstrate the applicability of our method, we have evaluated the MIM-VCD spectra for the stereoisomers of cryptophane-A, a large cage molecule with two cyclotriveratrylene bowls connected by three aliphatic linkers. Cryptophane molecules are among the first examples of synthetic "container molecules" that have been well-studied previously.[29,30] Together with a variety of bridging and substituent groups, several cryptophane molecules with varying cavity volume, aperture size, solubility, and recognition properties are possible. These molecular cages have the ability to encapsulate molecule-sized substrates completely. They are synthesized and studied primarily to understand the molecular recognition and encapsulation processes. Cryptophane-A is the first and simplest isomer belonging to this class of cage molecules.[29,30]

Both theoretically and experimentally, there has been a wide interest in studying the VCD spectrum of cryptophane-A. Optically pure cryptophane-A isomers have been recently synthesized through an optical resolution method.[31] From the theoretical point of view, evaluating the VCD spectrum of cryptophane-A ($C_{54}H_{54}O_{12}$), which has 120 atoms, can be computationally expensive, particularly when using large basis sets. Hence, theoretical investigation of the VCD spectra of species like cryptophane-A is still a challenging problem. Cryptophane-A may exist as either the *syn* or *anti* chiral diastereomer, the latter having D_3 symmetry. Since each of the O−C−C−O dihedral angles can be *trans* or *gauche*, there are many possible stereoisomers. However, it has been shown in previous work[28] that the D_3 isomer (also referred to as $T_1T_1T_1$) provides the best agreement with the experimental VCD spectra. (A schematic depiction of the structure of the enantiomers of the $T_1T_1T_1$ stereoisomer of cryptophane-A is provided in Figure 7.) Thus, we have considered only this isomer to predict the MIM2 spectrum and compare with experiment.

In previous work on cryptophane, the geometry optimization was carried out for the fragment representing two-thirds of the cage, and the entire molecule was then generated from this fragment.[28] In that work, it was clear that a polarized basis set, 6-31G(d), showed better agreement with the experiment than a smaller 3-21G basis set.[28] We have used the slightly larger 6-31+G(d,p) basis set containing diffuse functions in our analysis. Our geometry optimization was carried out for the entire molecule at MIM2, using MPW1PW91/6-31+G(d,p) as the high layer and the HF/6-31G as the low layer. The second layer used a smaller basis set, because of the size of the molecule and to explore the performance of MIM-VCD for large systems, where calculations with much larger basis sets may be computationally prohibitive. The calculations on cryptophane-

DOI: 10.1021/acs.jctc.5b00647
J. Chem. Theory Comput. XXXX, XXX, XXX−XXX

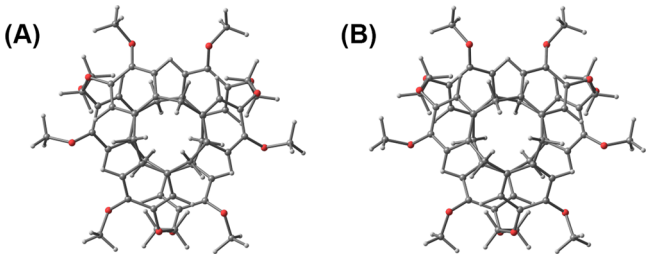

Figure 7. Enantiomers of the $T_1T_1T_1$ isomer of cryptophane-A, as viewed through the top C_3 symmetric axis: (A) (+)-enantiomer and (B) (−)-enantiomer. The optimized geometries are furnished in the Supporting Information. See the text for more details.

A at MIM2[MPW1PW91/6-31+G(d,p):HF/6-31G] required 1524 basis functions and 2490 primitive Gaussian functions. Optimizations, as well as IR and VCD spectral evaluations, are all carried out uniformly at the same level of theory. The full unfragmented calculations were not performed.

The theoretical spectra are evaluated in the gas phase and compared with the experiment conducted in $CDCl_3$ solvent. It has previously been confirmed that the solvent molecules do not alter the VCD spectrum of the parent $T_1T_1T_1$ isomers.[28] The VCD spectra in the 1000−1700 cm^{-1} region as seen in the experiment have been analyzed in the present work. Figure 8

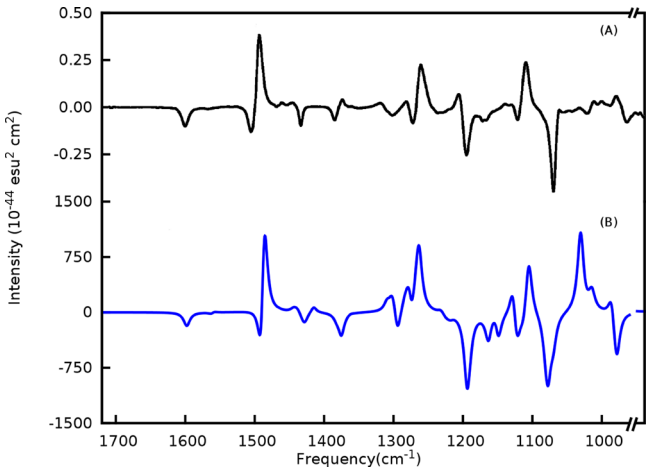

Figure 8. Comparison of (A) experimental with (B) MIM2-[MPW1PW91/6-31+G(d,p):MPW1PW91/6-31G] VCD spectra of (+)-$T_1T_1T_1$ stereoisomer of cryptophane-A. Coordinates and full VCD spectra are available in Table S3 in the Supporting Information. See the text for more details.

shows the experimental spectrum for cryptophane-A (top) with the MIM2 spectrum (bottom), using frequencies scaled by 0.952 and with a Lorentzian line shape with a width of 7.5 cm^{-1}. The full set of frequencies and VCD intensities are listed in Table S3 in the Supporting Information. The overall agreement between the MIM-VCD and the experimental spectra is very good, although there are some deviations in the lower frequency range (at ∼1000 cm^{-1}). The bands at 1607, 1577, and 1509 cm^{-1} correspond to the C═C stretching modes of the benzene rings. The next band between 1480 and 1420 cm^{-1} belongs to $-CH_2$ and $-CH_3$ deformation modes. The band at 1400−1250 cm^{-1} corresponds to coupled twisting and wagging modes of H−C−H bond. Symmetric and antisymmetric stretching modes of C−O−Me group occur at 1212−1034 cm^{-1}. The bands between 1183 and 1086 cm^{-1} are due to the aromatic C_{ring}−H deformations. Overall, the MIM2-VCD spectrum shows a good agreement with experiment for the D_3 stereoisomer. This suggests that MIM-VCD can be a powerful tool to assign VCD spectra for other large molecules in the future.

4. COMPARISON WITH PREVIOUS APPROACHES FOR LARGE MOLECULES

Because of the extensive demands on computational resources, the applicability of the direct approach to calculate VCD spectra for large molecules is still limited in the literature. Thus, approximate methods have been proposed to overcome these limitations.[32−36] Perhaps the most popular, and economical, alternative is the Cartesian Tensor Transfer Method (CTTM), and related approaches that have been widely applied to the calculation of VCD spectra for many large molecules.[37−39] While CTTM also obtains the second derivatives of the electronic energy (the Hessian matrix) as well as the intensities from the Hessian matrices and molecular property tensors calculated for smaller overlapping molecular fragments, there are significant differences from our MIM-VCD approach.

In the typical CTTM evaluation of the vibrational spectrum, all nearby Hessian matrix elements are selected from the fragments, and all long-range Hessian matrix elements are neglected. In addition, the first step is the construction of the relevant rotation matrix and finding the best fit of the fragments onto the parent molecule. The fit is performed by maximizing the overlap between two or three atoms in the fragments by least-squares optimization. This is done either by using a single rotation matrix or multiple rotation matrices for each pair of atoms. This may provide some ambiguity in their definitions, and the appropriate sum rules[40,41] may only be satisfied approximately.

Despite successful applications in reproducing the qualitative experimental spectra, some recent studies have questioned the accuracy and general applicability of CTTM.[42−44] Although large-sized fragments comprising about four amino acid residues were used, the ROA spectra obtained by the CTTM were found to be significantly deficient and errors up to 50 cm^{-1} in vibrational frequencies were observed. Generally, CTTM works best for systems with identical monomers such as polypeptides due to the repeating monomeric structure allowing for maximum overlaps.

Choi et al.[45,46] have proposed an approximate fragment method somewhat similar to the CTTM that does not require a repeating structural unit to be chosen as the translating fragment but instead uses a unit peptide fragment with two different chiral groups around the subject peptide bond. The unit fragment is translated along the polypeptide of interest and the Hessian matrix is filled. While this method was shown to be effective for the amide I band region, where the VCD intensities are strongly structurally dependent, many side chains and weak interactions are ignored.

In our MIM fragment-based method, many of these limitations are not applicable. The initial fragments and subsystems can be generated in a systematic manner without any assumptions or symmetry restrictions. We saturate all the dangling bonds with link hydrogen atoms. Later, the contribution of all of the link atoms in the subsystems are projected back onto the corresponding supporting and host atoms through a Jacobi projection method. This link atom projection contribution is carried out rigorously before constructing the full matrices and tensors. In addition, in the

DOI: 10.1021/acs.jctc.5b00647
J. Chem. Theory Comput. XXXX, XXX, XXX−XXX

two-layer MIM2 model, the long-range interactions are always considered at a low level of theory. In principle, the method can also be extended for multiple low-level correction layers. The vibrational frequencies of even large molecules can be evaluated precisely using this approach as shown previously for the calculation of the infrared spectra.[16] In addition, each fragment calculation is performed in the global coordinate frame; hence there are no errors resulting from the rotation and translation of the tensor elements while constructing the full molecular property tensors. In the present work, we have benchmarked the MIM-VCD method with two layers of theory and shown that the rotational strengths are calculated reliably.

Finally, the computational scaling of the MIM-VCD method with the size of the system in an important point. The sizes of the primary subsystems are the rate-limiting steps in these calculations. However, as the molecule gets larger, the number of primary subsystems grows linearly with the size of the system. Thus, the asymptotic scaling of MIM1 is linear. However, MIM2 also involves a calculation on the real system (full molecule) at the low level of theory. In most cases, this also has a tendency to be very efficient, but will be dependent on the high and low methods as well as the relative sizes of the basis sets used. Overall, the scaling advantage of the MIM-VCD increases dramatically as the system size increases. The effective performance of MIM-VCD for a large system such as cryptophane illustrates the computational advantage of such an approach. Substantially larger molecules can be investigated using our approach in the future.

5. CONCLUSIONS

Vibrational circular dichroism (VCD) is a powerful method for the determination of the absolute configurations of molecules. However, accurate evaluation of *ab initio* VCD spectra for large molecules can be computationally expensive, particularly in conjunction with large basis sets. In the present work, we have implemented and calibrated the MIM fragment-based method for evaluating VCD spectra of large molecules. The incorporation of the Jacobian link atom projection method as well as the employment of multiple layers of theory in accounting for long-range weak interactions are both important factors that contribute to the accuracy of the method. Our implementation of the algorithm is independent of the combination of levels of theory and fragmentation schemes, and the method is easily parallelizable without any severe modification to the algorithm. MIM-VCD is carefully benchmarked on a set of carbohydrate enantiomers. The frequencies and VCD intensities show an excellent agreement with the actual calculations. Larger systems such as perhydrotriphenylene and cryptophane-A have also been investigated, and the MIM-VCD spectra show very good correlation with the corresponding experimental spectra.

To evaluate the VCD spectra of even larger systems, the same algorithm can be extended readily using multiple layers of theory. Furthermore, the VCD spectrum can be very sensitive to the environment[47] and the spectra may show effects of solvents through chirality transfer effects.[48] This can only be addressed only by incorporating explicit solvent molecules into account while evaluating the VCD spectrum. Our MIM-VCD method may help us in incorporating the explicit solvent effects in an accurate and efficient manner. Overall, our MIM-VCD fragment-based approach significantly reduces the computational requirements and opens up a wide range of systems that can be studied through accurate *ab initio* methods.

ASSOCIATED CONTENT

Supporting Information

The Supporting Information is available free of charge on the ACS Publications website at DOI: 10.1021/acs.jctc.5b00647.

Cartoon illustrating the dimer- and trimer-based fragmentation schemes used for D-sucrose; MIM2 IR and VCD spectra of perhydrotriphenylene and the $T_1T_1T_1$ enantiomers of cryptophane-A; coordinates, energies, frequencies, and VCD intensities for the actual calculations of the initial benchmark set; MIM2 calculated results of perhydrotriphenylene; and MIM2 calculated results of (+)-$T_1T_1T_1$ cryptophane-A (PDF)

AUTHOR INFORMATION

Corresponding Author

*E-mail: kraghava@indiana.edu.

Notes

The authors declare no competing financial interest.

ACKNOWLEDGMENTS

Authors thank Professor Prasad Polavarapu for valuable suggestions and feedback. This work was supported by funding from NSF Grant No. CHE-1266154 at Indiana University. The authors also thank the Indiana University Big Red II supercomputing facility for computing time.

REFERENCES

(1) Keiderling, T. A. Vibrational Circular Dichroism Applications to Conformational Analysis of Biomolecules. In *Circular Dichroism and the Conformational Analysis of Biomolecules*; Fasman, G., Ed.; Springer: New York, 1996; pp 556−594.

(2) Nafie, L. A.; Dukor, R. K.; Freeman, T. B. Vibrational Circular Dichroism. In *Handbook of Vibrational Spectroscopy*; Chalmers, J. M., Griffiths, P. R., Eds.; Wiley: New York, 2002; pp 693−758.

(3) Polavarapu, P. L. *Ab initio* vibrational Raman and Raman optical activity spectra. *J. Phys. Chem.* **1990**, *94*, 8106−8112.

(4) Buckingham, A. D. Introductory lecture. The theoretical background to vibrational optical activity. *Faraday Discuss.* **1994**, *99*, 1−12.

(5) Nafie, L. A. Infrared and Raman vibrational optical activity: Theoretical and experimental aspects. *Annu. Rev. Phys. Chem.* **1997**, *48*, 357−386.

(6) Magyarfalvi, G.; Tarczay, G.; Vass, E. Vibrational circular dichroism. *Wiley Interdiscip. Rev. Comput. Mol. Sci.* **2011**, *1*, 403−425.

(7) Freedman, T. B.; Cao, X.; Dukor, R. K.; Nafie, L. A. Absolute configuration determination of chiral molecules in the solution state using vibrational circular dichroism. *Chirality* **2003**, *15*, 743−758.

(8) Stephens, P. J.; Lowe, M. A. Vibrational Circular Dichroism. *Annu. Rev. Phys. Chem.* **1985**, *36*, 213−241.

(9) Herrmann, C.; Reiher, M. In *Atomistic Approaches in Modern Biology*; Reiher, M., Ed.; Springer: Berlin, Heidelberg, 2007; Vol. *268*, pp 85−132.

(10) Ruud, K. *Ab Initio* Methods for Vibrational Circular Dichroism and Raman Optical Activity. In *Comprehensive Chiroptical Spectroscopy*; Berova, N., Polavarapu, P. L., Nakanishi, K., Woody, R. W., Eds.; Wiley: New York, 2012; pp 699−727.

(11) Polavarapu, P. L.; *Vibrational Spectra: Principles and Applications with Emphasis on Optical Activity*; Elsevier: Amsterdam, 1998.

(12) Stephens, P. J.; Devlin, F. J.; Pan, J.-J. The determination of the absolute configurations of chiral molecules using vibrational circular dichroism (VCD) spectroscopy. *Chirality* **2008**, *20*, 643−663.

(13) Stephens, P. J.; Devlin, F. J.; Cheeseman, J. R. *VCD Spectroscopy for Organic Chemists*; CRC Press: Boca Raton, FL, 2012.

DOI: 10.1021/acs.jctc.5b00647
J. Chem. Theory Comput. XXXX, XXX, XXX−XXX

(14) Gordon, M. S.; Fedorov, D. G.; Pruitt, S. R.; Slipchenko, L. V. Fragmentation methods: A route to accurate calculations on large systems. *Chem. Rev.* **2012**, *112*, 632−672.
(15) Mayhall, N. J.; Raghavachari, K. Molecules-in-Molecules: An extrapolated fragment-based approach for accurate calculations on large molecules and materials. *J. Chem. Theory Comput.* **2011**, *7*, 1336−1343.
(16) Jose, K. V. J.; Raghavachari, K. Evaluation of energy gradients and infrared vibrational spectra through Molecules-in-Molecules fragment-based approach. *J. Chem. Theory Comput.* **2015**, *11*, 950−961.
(17) Nafie, L. A. Adiabatic molecular properties beyond the Born-Oppenheimer approximation. Complete adiabatic wave functions and vibrationally induced electronic current density. *J. Chem. Phys.* **1983**, *79*, 4950−4957.
(18) Nafie, L. A.; Freedman, T. B. Vibronic coupling theory of infrared vibrational transitions. *J. Chem. Phys.* **1983**, *78*, 7108−7116.
(19) Nafie, L. A. Theory of vibrational circular dichroism and infrared absorption: Extension to molecules with low-lying excited electronic states. *J. Phys. Chem. A* **2004**, *108*, 7222−7231.
(20) Stephens, P. J. Gauge dependence of vibrational magnetic dipole transition moments and rotational strengths. *J. Phys. Chem.* **1987**, *91*, 1712−1715.
(21) Stephens, P. J. Theory of vibrational circular dichroism. *J. Phys. Chem.* **1985**, *89*, 748−752.
(22) Cheeseman, J. R.; Frisch, M. J.; Devlin, F. J.; Stephens, P. J. *Ab Initio* calculation of atomic axial tensors and vibrational rotational strengths using density functional theory. *Chem. Phys. Lett.* **1996**, *252*, 211−220.
(23) Cheeseman, J. R.; Frisch, M. J. Basis Set dependence of vibrational Raman and Raman optical activity intensities. *J. Chem. Theory Comput.* **2011**, *7*, 3323−3334.
(24) Stephens, P. J.; Devlin, F. J.; Aamouche, A. In *Chirality: Physical Chemistry*; ACS Symposium Series, Vol. *810*; American Chemical Society: Washington, DC, 2002; pp 18−33.
(25) Frisch, M. J.; Trucks, G. W.; Schlegel, H. B.; Scuseria, G. E.; Robb, M. A.; Cheeseman, J. R.; Scalmani, G.; Barone, V.; Mennucci, B.; Petersson, G. A.; Nakatsuji, H.; Caricato, M.; Li, X.; Hratchian, H. P.; Izmaylov, A. F.; Bloino, J.; Zheng, G.; Sonnenberg, J. L.; Hada, M.; Ehara, M.; Toyota, K.; Fukuda, R.; Hasegawa, J.; Ishida, M.; Nakajima, T.; Honda, Y.; Kitao, O.; Nakai, H.; Vreven, T.; Montgomery, J. A., Jr.; Peralta, J. E.; Ogliaro, F.; Bearpark, M.; Heyd, J. J.; Brothers, E.; Kudin, K. N.; Staroverov, V. N.; Kobayashi, R.; Normand, J.; Raghavachari, K.; Rendell, A.; Burant, J. C.; Iyengar, S. S.; Tomasi, J.; Cossi, M.; Rega, N.; Millam, M. J.; Klene, M.; Knox, J. E.; Cross, J. B.; Bakken, V.; Adamo, C.; Jaramillo, J.; Gomperts, R.; Stratmann, R. E.; Yazyev, O.; Austin, A. J.; Cammi, R.; Pomelli, C.; Ochterski, J. W.; Martin, R. L.; Morokuma, K.; Zakrzewski, V. G.; Voth, G. A.; Salvador, P.; Dannenberg, J. J.; Dapprich, S.; Daniels, A. D.; Farkas, Ö.; Foresman, J. B.; Ortiz, J. V.; Cioslowski, J.; Fox, D. J. *Gaussian 09, Revision D.01*; Gaussian, Inc.: Wallingford, CT, 2009.
(26) Dapprich, S.; Komáromi, I.; Byun, K. S.; Morokuma, K.; Frisch, M. J. A new ONIOM implementation in Gaussian98. Part I. The calculation of energies, gradients, vibrational frequencies and electric field derivatives. *J. Mol. Struct.: THEOCHEM* **1999**, *461−462*, 1−21.
(27) Stephens, P. J.; Devlin, F. J.; Schürch, S.; Hulliger, J. Determination of the absolute configuration of chiral molecules via density functional theory calculations of vibrational circular dichroism and optical rotation: The chiral alkane D3-anti-trans-anti-trans-anti-trans-perhydrotriphenylene. *Theor. Chem. Acc.* **2008**, *119*, 19−28.
(28) Brotin, T.; Cavagnat, D.; Dutasta, J.-P.; Buffeteau, T. Vibrational circular dichroism study of optically pure Cryptophane-A. *J. Am. Chem. Soc.* **2006**, *128*, 5533−5540.
(29) Brotin, T.; Dutasta, J.-P. Cryptophanes and their complexes—Present and future. *Chem. Rev.* **2009**, *109*, 88−130.
(30) Gabard, J.; Collet, J. Synthesis of a (D3)-bis-(cyclotriveratrylenyl) macrocage by stereospecific replication of a (C3)-subunit. *J. Chem. Soc., Chem. Commun.* **1981**, 1137−1139.
(31) Brotin, T.; Barbe, R.; Darzac, M.; Dutasta, J.-P. Novel Synthetic approach for optical resolution of Cryptophanol-A: A direct access to chiral Cryptophanes and their chiroptical properties. *Chem.—Eur. J.* **2003**, *9*, 5784−5792.
(32) Bouř, P.; Sopková, J.; Bednárová, L.; Maloň, P.; Keiderling, T. A. Transfer of molecular property tensors in cartesian coordinates: A new algorithm for simulation of vibrational spectra. *J. Comput. Chem.* **1997**, *18*, 646−659.
(33) Ghysels, A.; Van Neck, D.; Van Speybroeck, V.; Verstraelen, T.; Waroquier, M. Vibrational modes in partially optimized molecular systems. *J. Chem. Phys.* **2007**, *126*, 224102.
(34) Ghysels, A.; Van Neck, D.; Brooks, B. R.; Van Speybroeck, V.; Waroquier, M. Normal modes for large molecules with arbitrary link constraints in the mobile block Hessian approach. *J. Chem. Phys.* **2009**, *130*, 084107.
(35) Jiang, N.; Tan, R. X.; Ma, J. Simulations of Solid-State vibrational circular dichroism spectroscopy of (S)-Alternarlactam by using fragmentation quantum chemical calculations. *J. Phys. Chem. B* **2011**, *115*, 2801−2813.
(36) Thorvaldsen, A. J.; Gao, B.; Ruud, K.; Fedorovsky, M.; Zuber, G.; Hug, W. Efficient calculation of ROA tensors with analytical gradients and fragmentation. *Chirality* **2012**, *24*, 1018−1030.
(37) Andrushchenko, V.; Bour, P. Applications of the Cartesian coordinate tensor transfer technique in the simulations of vibrational circular dichroism spectra of oligonucleotides. *Chirality* **2010**, *22*, E96−E114.
(38) Andrushchenko, V.; Tsankov, D.; Krasteva, M.; Wieser, H.; Bour, P. Spectroscopic detection of DNA Quadruplexes by vibrational circular dichroism. *J. Am. Chem. Soc.* **2011**, *133*, 15055−15064.
(39) Bour, P.; Keiderling, T. A. Vibrational spectral simulation for peptides of mixed secondary structure: Method comparisons with the TrpZip model hairpin. *J. Phys. Chem. B* **2005**, *109*, 23687−23697.
(40) Polavarapu, P. L. An approximate relation for paramagnetic magnetizability emerging from the sum rules for Cartesian magnetic dipole moment derivatives. *Chem. Phys. Lett.* **1990**, *171*, 271−276.
(41) Polavarapu, P. L. Sum rules for Cartesian polarizability derivative tensors. *Chem. Phys. Lett.* **1990**, *174*, 511−516.
(42) Bieler, N. S.; Haag, M. P.; Jacob, C. R.; Reiher, M. Analysis of the Cartesian Tensor Transfer method for calculating vibrational spectra of polypeptides. *J. Chem. Theory Comput.* **2011**, *7*, 1867−1881.
(43) Yamamoto, S.; Bour, P. On the limited precision of transfer of molecular optical activity tensors. *Collect. Czech. Chem. Commun.* **2011**, *76*, 567−583.
(44) Yamamoto, S.; Li, X.; Ruud, K.; Bour, P. Transferability of various molecular property tensors in vibrational spectroscopy. *J. Chem. Theory Comput.* **2012**, *8*, 977−985.
(45) Choi, J.-H.; Cho, M. Amide I vibrational circular dichroism of dipeptide: Conformational dependence and fragment analysis. *J. Chem. Phys.* **2004**, *120*, 4383−4392.
(46) Choi, J.-H.; Kim, J.-S.; Cho, M. Amide I vibrational circular dichroism of polypeptides: Generalized fragmentation approximation method. *J. Chem. Phys.* **2005**, *122*, 174903.
(47) Polavarapu, P. L. Molecular structure determination using Chiroptical spectroscopy: Where we may go wrong? *Chirality* **2012**, *24*, 909−920.
(48) Sadlej, J.; Dobrowolski, J. C.; Rode, J. E. VCD spectroscopy as a novel probe for chirality transfer in molecular interactions. *Chem. Soc. Rev.* **2010**, *39*, 1478−1488.

DOI: 10.1021/acs.jctc.5b00647
J. Chem. Theory Comput. XXXX, XXX, XXX−XXX